Development/Plasticity/Repair

Distal Dendritic Inputs Control Neuronal Activity by Heterosynaptic Potentiation of Proximal Inputs

Edward B. Han and Stephen F. Heinemann
Salk Institute for Biological Studies, La Jolla, California 92037

Synapses onto distal dendritic tufts are believed to function by modulating time-locked proximal inputs; however, the role of these synapses when proximal inputs are asynchronous or silent is unknown. Surprisingly, we found that activation of apical tuft synapses alone resulted in heterosynaptic potentiation of proximal synapses. In mouse adult hippocampal CA1 pyramidal neurons, we show that activation of distal inputs from the entorhinal cortex (EC) specifically strengthens proximal synapses projecting from CA3. This slow AMPA receptor-mediated potentiation is accompanied by increased synaptic GluN2B-containing NMDA receptors, which are normally restricted to juvenile animals. These two synaptic modifications interact to generate striking bidirectional metaplastic changes. Heterosynaptically potentiated synapses become resistant to subsequent long-term potentiation (LTP) as the two forms of AMPA receptor-mediated potentiation occlude. However, this is only true when the LTP induction protocol is relatively weak. When it is strong and repeated, the magnitude of LTP after heterosynaptic plasticity is greatly increased, specifically through the activation of GluN2B-containing NMDA receptors. Thus, CA1 neurons expressing heterosynaptic potentiation induced by external sensory input from the EC become more strongly driven by internally generated environmental representations from CA3. Furthermore, subsequent SC LTP in this ensemble is shifted to potentiate only strongly activated CA3 inputs, while endowing these synapses with enhanced potentiation. These results show that one set of inputs can exert long-lasting heterosynaptic control over another, allowing the coupling of two functionally and spatially distinct pathways, thereby greatly expanding the repertoire of cellular and network plasticity.

Introduction

Synaptic currents originating in the apical dendritic tuft are greatly attenuated by electrotonic decay, and even distal dendritic spikes evoked by the strong simultaneous activation of tuft synapses are unable to reliably drive somatic action potentials (APs) (Schiller et al., 1997; Golding and Spruston, 1998; Jarsky et al., 2005). Distal dendritic signals can interact with coincident proximal inputs to either boost or inhibit activity, but this modulation requires coactivation of both pathways within a narrow time window (Larkum et al., 1999; Remondes and Schuman, 2002; Dudman et al., 2007; Takahashi and Magee, 2009). Thus, it remains unclear how, or even if, distal synapses can impact neuronal function when proximal input is not coincident or absent.

We studied this question in the output layer of the hippocampus, CA1, which receives two well-segregated synaptic inputs carrying two distinct types of information. Entorhinal cortical inputs synapse on the distal apical tuft and carry path integration signals such as grid cell firing from the medial entorhinal cortex (Sargolini et al., 2006) as well as nonspatial information from the lateral entorhinal cortex (Hargreaves et al., 2005). Schaffer collateral (SC) synapses from hippocampal CA3 innervate the proximal apical and basal dendrites and carry internally generated spatial maps.

Previous studies suggest that the direct entorhinal cortical inputs onto the distal apical tuft have the unusual ability to heterosynaptically control synaptic plasticity at distant SC synapses. These studies activated tuft synapses at low frequency (1 Hz for 900 s) and found intriguing, though somewhat contradictory, results. One study found that low-frequency stimulation produced heterosynaptic potentiation at SC synapses (Wöhrl et al., 2007), whereas another found that the same stimulation protocol did not affect basal synaptic strength at SC synapses, but rather depotentiated previously potentiated SC synapses (Izumi et al., 2008). Rather than using low-frequency stimulation, we used high-frequency activation, similar to the firing of these afferents *in vivo* (Fyhn et al., 2008), to investigate how entorhinal cortical inputs may control SC synapses.

Using a combination of slice electrophysiology and calcium imaging, we found that activation of dendritic tuft synapses resulted in the long-lasting modification of proximal apical synapses, by both potentiating AMPA receptor-dependent synaptic transmission and increasing the contribution of synaptic GluN2B, the predominant NMDA receptor subunit in juvenile animals. As a result, SC synapses in the apical dendrite are strengthened but also shift their input selectivity to specifically potentiate strong afferents from CA3 via the activation of GluN2B.

Materials and Methods

Slice preparation. Horizontal hippocampal slices (400 μm) were made from young male adult C57/BL6 mice (aged 6–15 weeks for field record-

Received July 5, 2012; revised Nov. 6, 2012; accepted Nov. 10, 2012.

Author contributions: E.B.H. and S.F.H. designed research; E.B.H. performed research; E.B.H. analyzed data; E.B.H. and S.F.H. wrote the paper.

This work was supported by an NIA training grant (E.B.H.) and an NIH Blueprint grant (S.F.H.). We thank Nelson Spruston, Massimo Scanziani, and Martha Bagnall for their generous advice and critical reading of this manuscript; Nelson Spruston for financial support; and Jeffry Isaacson and Gabrielle Edgerton for comments.

Correspondence should be addressed to Edward B. Han at his present address: Northwestern University, 2205 Tech Drive, Hogan 2160, Evanston, IL 60208. E-mail: edbhan@gmail.com.

DOI:10.1523/JNEUROSCI.3219-12.2013

 0270-6474/13/331314-12$15.00/0

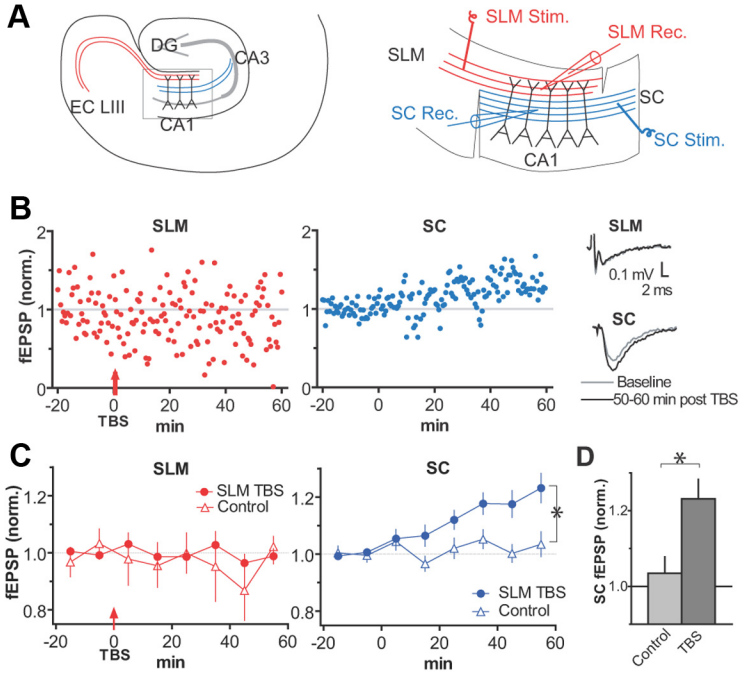

Figure 1. Activation of SLM inputs potentiates apical SC synapses. ***A***, Left, Schematic of inputs to CA1. Right, Slice and electrode placement after removal of the dentate gyrus (DG) and CA3. Small cuts are made proximal to both stimulating electrodes to prevent possible cross-stimulation of pathways. EC LIII, Layer III of the entorhinal cortex. ***B***, Sample experiment in one slice. At time 0, TBS (red arrow) is delivered to the SLM pathway only. Right, Average traces of fEPSPs in SLM and SC at baseline (−20 to 0 min) and 50–60 min after SLM TBS. ***C***, Mean of normalized fEPSPs (±SEM) averaged across all slices for SLM (left) and SC (right; $*p < 0.05$). ***D***, Average of fEPSPs 50–60 min after TBS (or no TBS control), normalized to baseline.

ings and 6–8 weeks for whole-cell recordings), in compliance with the animal use and care guidelines of the Salk Institute. Slicing was done on a Leica VT1200S in ice-cold sucrose-substituted artificial cerebrospinal fluid (ACSF) containing the following (in mM): 25 $NaHCO_3$, 3 KCl, 85 NaCl, 1.25 NaH_2PO_4, 75 sucrose, 25 glucose, 0.5 sodium ascorbate, 0.5 $CaCl_2$, and 4 $MgCl_2$. Slices recovered at 32–33°C for 1.5 h in recording ACSF containing (in mM): 25 $NaHCO_3$, 3 KCl, 125 NaCl, 1.25 NaH_2PO_4, 25 glucose, 1.3 $CaCl_2$, and 1 $MgCl_2$, and then held at room temperature. Slices were microdissected before recording by removing the dentate gyrus and CA3 and making small cuts in the stratum lacunosum moleculare (SLM) and SC to isolate stimulation of the SC and SLM pathways (Fig. 1*A*).

Electrophysiology. Recordings were performed at 32–33°C at least 3 h after slicing since baseline synaptic strength is not completely stable at earlier times. Concentric bipolar electrodes delivered electrical stimulation (100 μs duration) at 0.0167 or 0.0333 Hz. For extracellular field potential recordings, recording pipettes ranged from 1 to 3 MΩ and were filled with ACSF. SLM stimulation intensity was set at 40–50% of maximal field EPSP (fEPSP) peak, and the same intensity was used to deliver SLM theta-burst stimulation (TBS). Slices with a half-maximal SLM fEPSP smaller than 0.1 mV were not used. SC stimulation was set so fEPSP peak was 0.3–0.4 mV. For whole-cell experiments, borosilicate glass pipettes ranged from 2 to 4 MΩ.

For repatch experiments, intracellular recording solution contained the following (in mM): 140 K^+-gluconate, 10 NaCl, 10 HEPES, 0.1 EGTA, 3 MgATP, 0.3 LiGTP, 10 phosphocreatine-Tris, and 0.05 Alexa 555, pH 7.24, osmolarity 310–320. Baseline recordings (5 min duration) began 10 min after break in and were performed in voltage clamp with the cell held at the calculated Cl^- reversal potential (−67 mV) after correcting for the calculated liquid junction potential (15.4 mV). After pulling off the cell, we waited at least 20 min before delivering an SLM TBS to allow the cell to recover from patching. Alexa-filled neurons were targeted for repatch one to three times to obtain a satisfactory series resistance, R_s (±20% of baseline R_s, all recordings, <20 MΩ). BAPTA experiments were done with the same methodology except internal solution substituted 5 mM BAPTA-tetrapotassium salt for EGTA, and K^+-gluconate was lowered to 115 mM.

For loose-patch experiments, SLM and SC field stimulation intensity was set as described above for extracellular field recordings. We whole-cell patched a CA1 pyramidal neuron, recorded EPSCs, and pulled off the cell, as described for repatching. We then loose-patched the same CA1 pyramidal neuron using a borosilicate glass pipette (2–4 MΩ) filled with external solution. We continuously monitored membrane resistance, capacitance, and series resistance to ensure that we did not accidentally break into the cell. We never spontaneously broke into a cell while loose patched. To verify the quality of recording, we looked for high signal-to-noise capacitative transients representing APs by first giving a short train of three SC stimuli at 100 Hz. If we did not see an evoked AP, we simply waited to observe a spontaneous AP. Then we delivered a typical SLM TBS (10 stimuli at 100 Hz, repeated 10 times at 5 Hz) to look for somatic spikes. In three neurons, after recording the SLM TBS in loose-patch configuration, we pulled off the loose patch and waited >60 min to allow expression of heterosynaptic plasticity. Then we repatched the same neuron and measured the SC EPSC.

For AMPA/NMDA EPSC ratio recordings, heterosynaptic potentiation was induced while recording fEPSPs. Approximately 60 min after SLM TBS (or controls), we washed in 6-Imino-3-(4-methoxyphenyl)-1(6H)-pyridazinebutanoic acid hydrobromide (SR95531; 10 μM; Ascent Scientific) and patched a neuron [internal solution contained (in mM) 140 Cs^+-gluconate, 10 CsCl, 10 HEPES, 0.5 EGTA, 3 MgATP, 0.3 LiGTP, and 10 phosphocreatine-Tris, pH 7.24, with osmolarity 310–320]. After 10 min, we recorded AMPA receptor-mediated currents in voltage clamp at −70 mV for 10 min at one stimulation per minute. Stimulation intensity was set so EPSCs were 100–200 pA. Then we washed in NBQX (10 μM; Ascent Scientific), held the cell at +30 mV, and recorded NMDA receptor-mediated currents at one stimulation per minute. AMPA/NMDA ratios were calculated using EPSC peaks. For measuring ifenprodil sensitivity, after 10 min of baseline recording of NMDA receptor-mediated currents, we washed in ifenprodil (3 μM; Tocris Bioscience) for 35 min, then measured the NMDA receptor-mediated EPSC for 15 min, then washed in D,L-APV (100 μM; Ascent Scientific). Only experiments where R_s was low and stable were analyzed (±20% of baseline R_s; all recordings, <20 MΩ). For all experiments using ifenprodil (see Figs. 8, 9), we used paired-pulse stimulation with a 50 ms interval to accelerate GluN2B block by the use-dependent ifenprodil (Barria and Malinow, 2005). Only the first pulse was measured for the experiments shown. For experiments looking at metaplasticity, SC stimulus intensity was turned down after heterosynaptic potentiation so fEPSPs were approximately the same size as before potentiation. For field experiments examining SC LTP after heterosynaptic plasticity (see Fig. 7), we stimulated two independent SC pathways in each slice. For quantification of heterosynaptic plasticity, we averaged both SC pathways, since the expression of heterosynaptic plasticity is not input specific. Subsequent SC LTP was induced in one pathway, and the resulting synaptic strength was normalized to the naive pathway.

Calcium imaging. SLM and SC field stimulation intensity was set as described above for extracellular field recordings. We then whole-cell patched a neuron with a pipette containing K^+-gluconate internal and 20 μM Alexa 555, with either 100–200 μM Oregon Green BAPTA-1 (OGB-1) or 200 μM Fluo-5F. We allowed dye to fill distal dendrites of the neuron for 50–60 min before imaging. Images near the stratum radiatum (SR)/SLM were collected 40× magnification at 30 Hz with a cooled

CCD camera (Andor iXon DU885) triggered by pClamp to synchronize imaging with electrophysiology. Excitation light was supplied by an Exfo Xcite system. The approximate border between the SR and SLM was identified based on the dark appearance of the SLM due to the myelinated fibers projecting from the entorhinal cortex.

Data acquisition and analysis. Recordings were obtained with a Multiclamp 700B (Molecular Devices) under the control of pClamp (Molecular Devices), filtered at 2 kHz and digitized at 10 kHz by a Digidata (Molecular Devices). All data analysis was performed in Matlab, Excel, and Prism. For calcium imaging, data were analyzed using custom-written Matlab routines. Regions of interest along the apical dendrite were selected, and three nearby background regions were averaged and used to subtract baseline fluorescence before calculating the $\Delta F/F$. Average values are means ± SEM. Statistical comparisons were made using nonparametric tests: Mann–Whitney for pairwise comparisons, and Kruskal–Wallis with a *post hoc* Dunn's multiple comparison as indicated in the text.

Results

Initial demonstration of heterosynaptic potentiation

We recorded from acute hippocampal slices from young adult mice (6–15 weeks) that were microdissected to allow independent stimulation of the distal dendritic pathway in SLM and proximal pathway in stratum radiatum (Fig. 1*A*) (Remondes and Schuman, 2002). Stimulation in the SLM activates perforant path fibers originating in layer III of the entorhinal cortex and a smaller projection from the thalamic reuniens (Wouterlood et al., 1990; Otmakhova et al., 2002; Remondes and Schuman, 2002), whereas stimulation in the stratum radiatum activates SC axons from CA3 of the hippocampus. Inhibition was intact, and recordings performed at 32–33°. We monitored synaptic transmission by measuring the initial slope of the extracellular fEPSP, which reports AMPA-receptor mediated synaptic strength.

Theta-burst stimulation of the SLM (five stimuli at 100 Hz, repeated 10 times at 5 Hz, set at 40–50% of maximal intensity) had no long-lasting effect on SLM synaptic strength compared to control slices that did not receive a TBS (measured at 50–60 min after TBS and normalized to −20–0 min baseline; controls 1.02 ± 0.04, $n = 7$; TBS, 0.99 ± 0.03, $n = 11$; $p = 0.47$; Fig. 1*B*, *C*, left). In contrast, the SC pathway exhibited a slow increase in synaptic transmission (controls, 1.04 ± 0.04, $n = 7$; TBS, 1.23 ± 0.05, $n = 11$; $p < 0.05$; Fig. 1*B–D*). Synaptic strength in the SC pathway was unchanged immediately after SLM TBS, indicating no posttetanic potentiation at SC synapses, suggesting that SC axons were not cross-stimulated by the SLM stimulating electrode (Fig. 1*B*, *C*). See Figure 5 for more details on the pathway-specificity of SLM stimulation.

Further characterization of heterosynaptic potentiation

This exclusively heterosynaptic potentiation of SC synapses was restricted to the apical dendrite as two-pathway experiments in the SR and stratum oriens (SO) showed significant potentiation in only the SR pathway (SR with SLM TBS, 1.28 ± 0.03, $n = 5$, $p < 0.01$; SO with SLM TBS, 1.01 ± 0.03, $p = 0.66$; Fig. 2*A*). Heterosynaptic potentiation was not caused by test pulses in either the SLM or SC (no SLM test pulses, 1.34 ± 0.09, $n = 3$ vs with SLM test pulses, 1.23 ± 0.05, $n = 11$; $p = 0.29$; potentiation of SC pathway stimulated with test pulses throughout experiment, 1.31 ± 0.03, $n = 4$ vs SC pathway with test pulses shut off until 50–60 min after TBS, 1.47 ± 0.08, $n = 4$; $p = 0.26$, Fig. 2*C*). Finally we investigated the pathway specificity of the induction of heterosynaptic potentiation. Is SLM stimulation required for heterosynaptic plasticity or can it be induced by SC synapses? One unusual aspect of the SLM TBS we use to induce heterosynaptic potentiation is that it is too weak to produce homosynaptic LTP at SLM synapses (Fig. 1*B*, *C*, left). Perhaps stimulation that is subthreshold for LTP is sufficient to induce heterosynaptic potentiation. To test this hypothesis, we delivered a weak TBS to one SC pathway and looked for heterosynaptic potentiation in an independent SC pathway. Administering a TBS protocol subthreshold for inducing homosynaptic LTP to one SC pathway (three stimuli at 100 Hz, repeated eight times at 5 Hz) did not produce heterosynaptic potentiation in an independent SC pathway (at 30–40 min after TBS, stimulated SC pathway, 0.99 ± 0.06, $n = 5$; no TBS SC pathway, 0.93 ± 0.05, $n = 5$; $p = 0.54$; Fig. 2*D*). We also note that suprathreshold (i.e., producing LTP) stimulation of one SC pathway does not produce heterosynaptic potentiation in an independent SC pathway (Fig. 7*B*). To summarize, heterosynaptic potentiation at SC synapses in response to SLM stimulation is restricted to the apical dendrite and does not spread to basal dendrites, does not depend on continuous test stimulation in either the SLM or SC pathway, and cannot be produced by stimulation of SC synapses that is subthreshold for LTP induction.

Heterosynaptic potentiation measured in single neurons

These experiments were done using extracellular field recordings that average signals from many local synapses; however, what is the response of individual neurons? There are two possibilities: (1) no potentiation in some cells averaged with large potentiation in others, or (2) uniform potentiation across the population. To distinguish between these possibilities, we turned to whole-cell patch clamp. To prevent washout of LTP, we developed a whole-cell repatching technique that allows for low series resistance (R_s) recording (in contrast to perforated-patch recordings), while limiting dialysis of intracellular components (Fig. 3*A*). Cells were patched with a K^+-gluconate-based internal solution containing Alexa 555 to label the cell and held at Cl^- reversal potential in voltage clamp to record responses to SC stimulation. After recording baseline EPSCs, the pipette was gently pulled off the cell, allowing the membrane to reseal. After a 20 min interval to allow the cell to recover from patching, slices either received SLM TBS or no stimulation (controls). Approximately 60 min later, to allow expression of plasticity, the same cell was targeted for repatch and EPSCs measured again. Only recordings where the R_s was stable within ±20% between the initial patch and repatch were included. There was no difference in the initial R_s of control and SLM TBS neurons (controls, 10.99 ± 0.81 MΩ, $n = 6$; SLM TBS, 12.21 ± 1.01 MΩ, $n = 8$; $p = 0.57$; Fig. 3*D*, inset). In addition, we also monitored the extracellular field potential in the same slice, allowing us to compare potentiation in a single cell versus the rest of the population.

Control neurons showed no change in the SC EPSC after repatching (sample experiment in Fig. 3*B*), verifying the stability of the repatch technique (control EPSC, 1.03 ± 0.05, $n = 6$; control fEPSP, 1.10 ± 0.10, $n = 6$; Fig. 3*D*, open triangles). In contrast, most neurons that received SLM TBS showed significant SC potentiation (sample experiment in Fig. 3*C*; TBS EPSC, 1.41 ± 0.11, $n = 8$, $p < 0.05$ compared to control EPSC; TBS fEPSP, 1.42 ± 0.09, $n = 8$, $p < 0.05$ compared to control fEPSP; Fig. 3*D*, open circles). Plotting response amplitude in the patched neuron versus the potentiation in the population revealed a good correspondence between the averaged single-cell and population data (Fig. 3*D*). Thus, we conclude that heterosynaptic potentiation is not restricted to a subset of cells, but rather occurs in a majority of neurons in the population. We note that in this experiment we failed to induce heterosynaptic plasticity in a relatively high per-

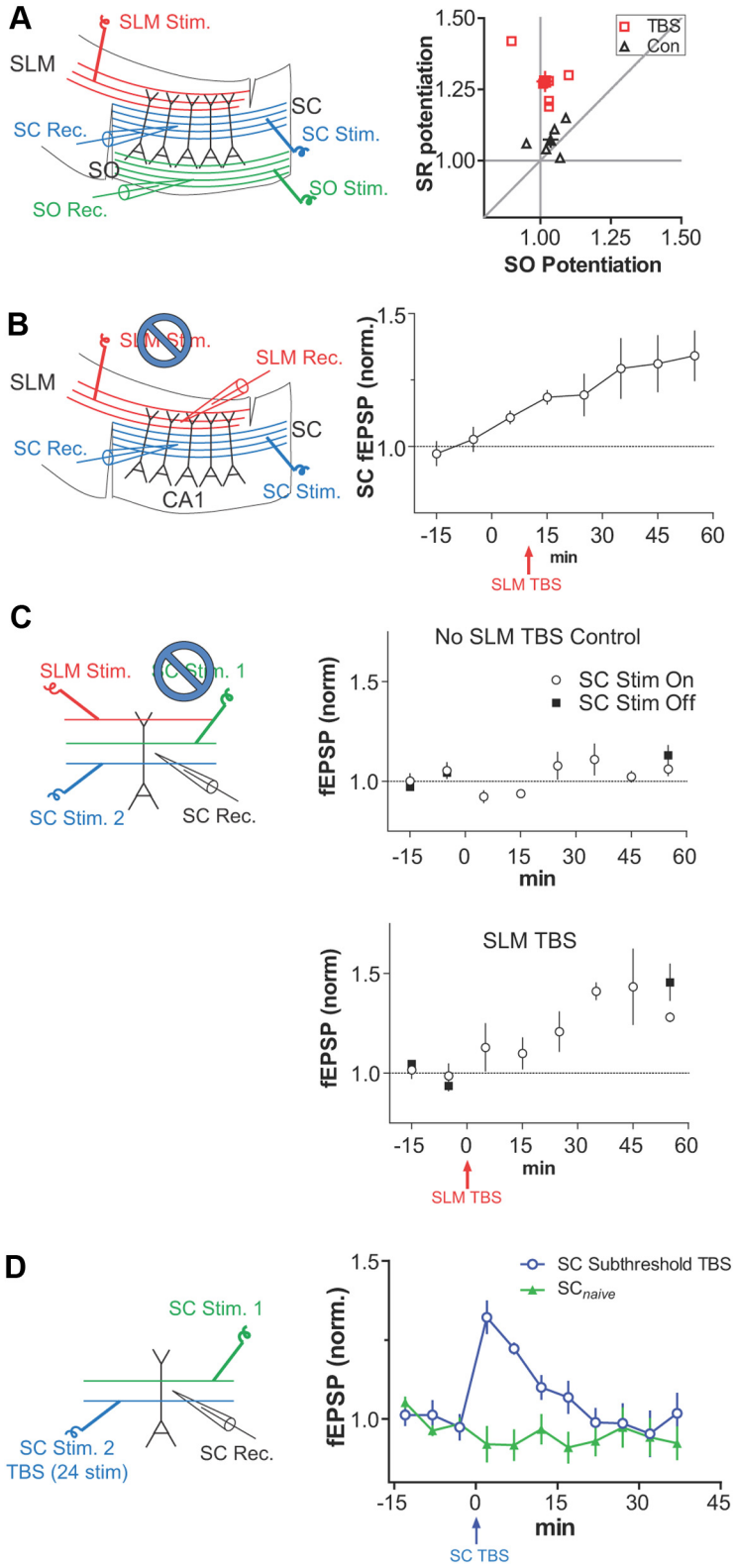

Figure 2. Further characterization of heterosynaptic potentiation. ***A***, Heterosynaptic potentiation is restricted to the stratum radiatum. Left, Schematic of electrode placement. Right, Scatter plot of potentiation of SO potentiation versus SR potentiation in each slice (open symbols) and average of all SO potentiation versus SR potentiation (closed symbols). ***B***, Heterosynaptic potentiation does not require SLM test stimulation. Left, Schematic of electrode stimulation. SLM electrode intensity is set and then used only to give SLM TBS (black arrow). Right, SC fEPSP after SLM TBS with no SLM test pulses. ***C***, Heterosynaptic potentiation does not require SC test stimulation. Left, Schematic of electrode stimulation. SC1 stimulation is given only during baseline, then shut off until the end of the experiment. Top right, Control experiment with no SLM TBS. Bottom right, SC fEPSP in stimulated and nonstimulated pathways after SLM TBS. ***D***, SC TBS subthreshold for inducing homosynaptic LTP does not produce heterosynaptic potentiation in an independent SC pathway. Three SC stimuli given at 100 Hz repeated eight times at 5 Hz does not produce homosynaptic LTP or heterosynaptic potentiation or at unstimulated SC synapses.

centage of slices (2 of 8, or 25%), in which case both the fEPSP and EPSC remained near baseline levels. This failure rate is somewhat higher than that observed in experiments with only extracellular recordings (~10%). This is likely because in extracellular recording-only experiments, we continuously monitor SLM field strength before taking the baseline and are able to turn up stimulation strength in case the SLM fEPSP falls below 40% of maximal. For experiments using whole-cell patch, we set the SLM stimulation strength using field recording, but then switch to using that manipulator for patching a cell, so we are unable to monitor SLM field strength just before taking baseline synaptic strength measurements. Thus, the failure to induce heterosynaptic plasticity in some slices is likely due to subthreshold stimulation of distal dendritic synapses.

Role of intracellular Ca^{2+}

Within an individual neuron, elevated Ca^{2+} is a common trigger for synaptic plasticity (Malenka et al., 1988). To probe the role of cell-autonomous Ca^{2+} signaling, we used the repatch technique to specifically load only patched neurons with the Ca^{2+} chelator BAPTA (5 mM) during the baseline recording period. Indeed we found that BAPTA blocked heterosynaptic plasticity in loaded cells (control BAPTA EPSC, 1.07 ± 0.08, $n = 5$ vs TBS BAPTA EPSC, 1.05 ± 0.12, $n = 4$; $p = 1$; Fig. 3*E*), while the remaining population of unloaded neurons in the same slice displayed normal potentiation (control fEPSP, 1.15 ± 0.05, $n = 5$ vs TBS fEPSP, 1.61 ± 0.17, $n = 4$; $p < 0.05$; Fig. 3*E*,*F*). There was no difference in the initial R_s of control and SLM TBS neurons (controls, 14.71 ± 1.31 MΩ; SLM TBS, 10.87 ± 1.05 MΩ; $p = 0.29$; Fig. 3*F*, inset). These results indicate that cell-autonomous Ca^{2+} signaling is required for heterosynaptic potentiation.

Role of somatic APs

One way SLM activation could elevate neuronal calcium is by evoking somatic action potentials. To assess the role of somatic APs in triggering heterosynaptic plasticity, we used a variant of the repatch technique. First we whole-cell patched a neuron, recorded EPSCs, and pulled the pipette off the cell, identical to a repatch experiment. Then we brought in a pipette filled with ACSF and loose patched the same cell. In this configuration, the pipette tip is nestled up against the cell, but not broken through the membrane, al-

lowing the recording of APs as capacitative transients without disturbing the intracellular contents of the cell. To verify the quality of the recording, we tried to evoke an AP with three stimulations of the SC pathway at 100 Hz. If that did not evoke an AP, we waited for a spontaneous AP to gauge recording quality. All recordings showed APs with a high signal-to-noise ratio (Fig. 4*A*). None of the recorded neurons exhibited spiking in response to SLM TBS (0/18; Fig. 4*B*,*C*). We repatched three of the 18 neurons, verifying that they were still healthy, and showed normal heterosynaptic potentiation (1.45 ± 0.16, $n = 3$; Fig. 4*D*). These data indicate that somatic APs are not required for the induction heterosynaptic plasticity.

Spatial extent of Ca^{2+} influx during SLM TBS stimulation

Together, our data suggest that stimulation of distal tuft synapses generates Ca^{2+} transients required for heterosynaptic potentiation. These Ca^{2+} transients could produce potentiation in SC synapses in one of two ways: (1) transients are spatially restricted to the SLM region and active a long-range signaling cascade targeted at distant SC synapses or (2) transients generated in the SLM extend into the SR, producing direct calcium-mediated potentiation at SC synapses. To distinguish between these two possibilities, we directly measured the spatial extent of Ca^{2+} influx during SLM TBS using Ca^{2+} imaging. We patched a CA1 neuron, filling with either OGB-1 (100–200 μM, $n = 6$; Fig. 5*A*) or Fluo-5F (200 μM, $n = 3$), and allowed dye to load distal dendrites of the neuron for 50–60 min before imaging. We marked the approximate SLM/SR border based on the dark appearance of the myelinated axons from the entorhinal cortex versus the phase bright axons from CA3. We imaged a section of the apical dendrite straddling the SLM/SR border and recorded both Ca^{2+}-induced fluorescence signals and membrane potential (V_m) in current clamp. We found that SLM TBS generated large Ca^{2+} transients that were largely restricted to the distal apical tuft (Fig. 5*B*, top left). The simultaneously recorded somatic V_m showed a very modest depolarization (Fig. 5*B*, bottom left), consistent with our earlier finding that SLM stimulation does not generate somatic APs (Fig. 4). As a positive control for detecting fluorescence changes in the proximal apical dendrite, we also gave a short burst of SC stimulation resulting in a backpropagating AP (bAP; Fig. 5*B*, bottom right). Ca^{2+} transients associated with the bAP were easily detectible throughout the apical dendrite (Fig. 5*B*, top right). Pooled data from all slices fit with a fourth-order polynomial ($R^2 = 0.65$) show that the maximal intracellular Ca^{2+} signal in response to SLM stimulation decreased dramatically at the SLM/SR border (Fig. 5*C*). To verify that the *dF/F* reported by the high-affinity Ca^{2+} sensor OGB-1 ($K_d = 170$ nM) was not decreased by Ca^{2+} saturation, we compared OGB-1 measurements to the low-affinity sensor Fluo-5F ($K_d = 2300$ nM). We binned the *dF/F* for each analysis window measured from 20 μm within the SLM to the putative SLM/SR border and compared the two sensors. There was no difference in the *dF/F* reported by the two sensors (OGB-1, 12.02 ± 2.49%, $n = 8$ analysis windows from six neurons vs Fluo-5F, 6.95 ± 2.03%, $n = 5$ from three neurons), nor was there a difference in the mean position of the analysis windows between the two sensors (OGB-1, −7.09 μm ± 2.46 from the SLM/SR border, $n = 8$ vs Fluo-5F, −8.31 μm ± 2.89, $n = 5$), indicating that OGB-1 was not appreciably saturated by Ca^{2+} binding. These data rule out direct calcium influx at SC synapses and suggest a long-distance signaling pathway induced in the SLM and directed to SC synapses. We also note that these data showing no Ca^{2+} elevation in the SR, together with the lack of

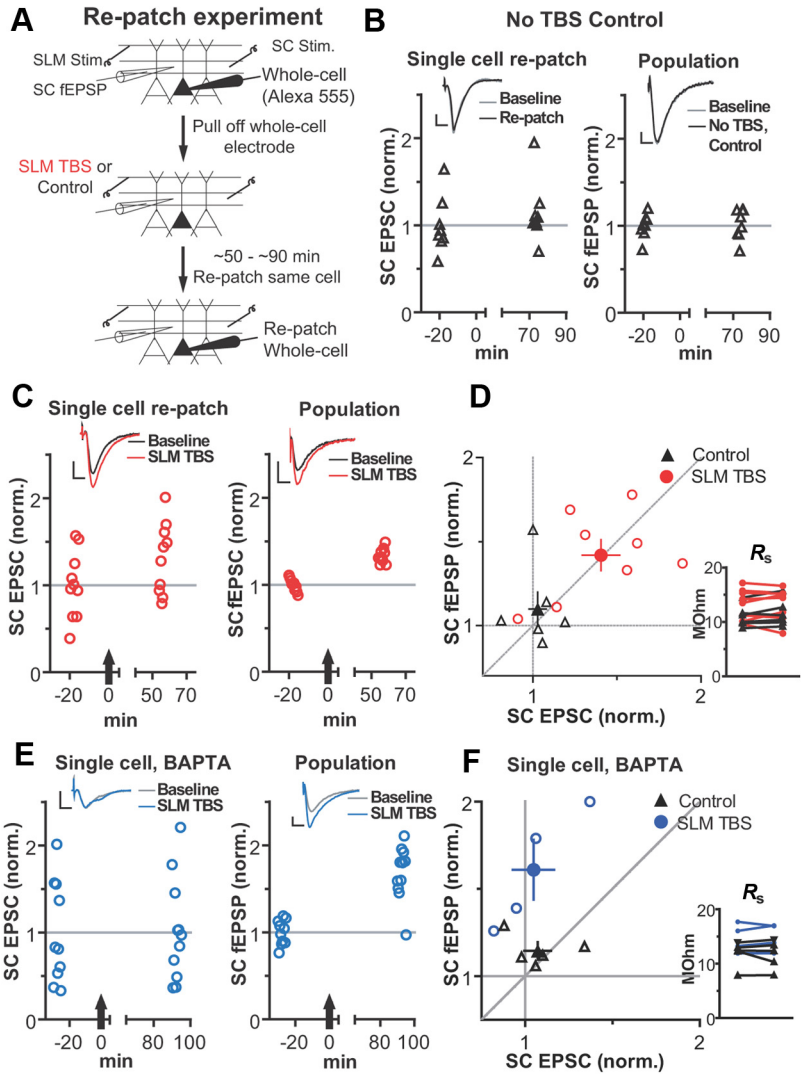

Figure 3. Heterosynaptic potentiation measured in single neurons. ***A***, Schematic of repatch experiment. Five minutes of baseline EPSCs are recorded in whole-cell voltage clamp (cell held at Cl^- reversal potential). SLM TBS is given ~20 min after pulling the electrode off the cell. The same cell is repatched after the expression of plasticity, and EPSCs measured again. ***B***, Sample control experiment showing SC EPSC (left) in a repatched cell and the simultaneously recorded fEPSP (right). Inset, Average traces. ***C***, Sample experiment in a slice receiving SLM TBS (black arrow). ***D***, Scatter plot of potentiation of EPSC versus fEPSP in each experiment (open symbols) and average of all control versus SLM TBS experiments (closed symbols). Inset, R_s values of whole-cell recordings at baseline and repatch. ***E***, Sample experiment in a single neuron filled with BAPTA (5 mM, left) and the population (right). Calibration: Insets, ***B***, ***C***, ***E***, EPSC, 50 pA, 5 ms; fEPSP, 0.2 mV, 5 ms. ***F***, Scatter plot of all experiments (open symbols) and average of all control and SLM TBS experiments (closed symbols).

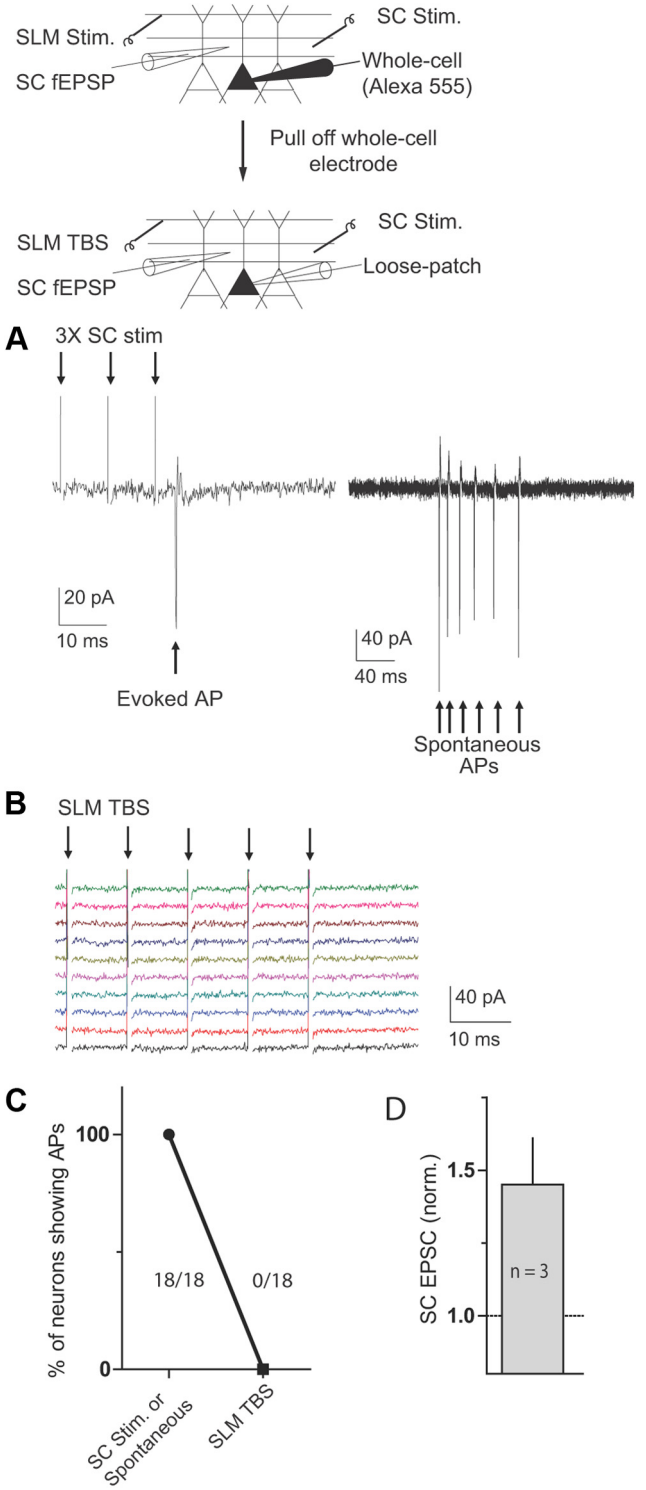

Figure 4. Somatic APs not required for heterosynaptic potentiation. Cells were patched, and baseline EPSCs were recorded to maintain consistency with previous repatch experiments. After pulling off the pipette and allowing the neurons to recover, they were recorded in loose-patch configuration. ***A***, Seal quality was tested by trying to evoke a spike using 3× SC stimulation at 100 Hz (left). Stimulus artifacts are marked by down arrows, and a clear capacitative transient corresponding to a somatic spike is marked with an up arrow. If synaptic stimulation failed to evoke a spike, we waited to record a spontaneous spike (right) to verify recording quality. ***B***, Same cell as in the middle panel, loose-patch recording during SLM TBS. No APs are seen, only stimulus artifacts. ***C***, Left, Summary of APs detected during SLM TBS. ***D***, In three of the neurons shown in ***C***, we repatched the neuron ~60 min after SLM TBS and compared the SC EPSC to baseline to confirm cell health and the normal expression of heterosynaptic plasticity.

post-tetanic potentiation at SC synapses in response to SLM TBS (Fig. 1*B*), illustrate that the SLM stimulation used for generating heterosynaptic potentiation is restricted to SLM synapses and does not produce significant direct activation of SC synapses.

Signaling pathways required for the induction of heterosynaptic potentiation

Next we investigated the signaling pathways required for heterosynaptic potentiation. NMDA receptors play a critical role in the induction of many forms of synaptic plasticity (Morris et al., 1986). We found that blocking NMDA receptors with D,L-APV (100 μM) or 3-((*R*)-2-carboxypiperazin-4-yl)-propyl-1-phosphonic acid (*R*-CPP; 100 μM) did not significantly inhibit heterosynaptic potentiation (1.17 ± 0.03, $n = 5$, $p > 0.05$ compared to TBS; Fig. 6*A*,*E*). Instead, previous studies have implicated R-/T-type Ca^{2+} channels in the induction of synaptic plasticity evoked by distal dendritic stimulation (Golding et al., 2002; Takahashi and Magee, 2009). Indeed we found that blocking R-/T-type Ca^{2+} channels with NiCl (50 μM) completely prevented heterosynaptic potentiation (0.99 ± 0.04, $n = 5$; $p < 0.05$ compared to TBS; Fig. 6*B*,*E*), without affecting basal synaptic transmission in the SLM pathway.

Next we examined the role of $GABA_A$ receptor-mediated inhibition on heterosynaptic potentiation. In contrast to homosynaptic LTP which does not require inhibition, we found that blocking $GABA_A$ receptors throughout the experiment with SR95531 (3 μm) prevented heterosynaptic potentiation (1.00 ± 0.04, $n = 3$, $p > 0.05$; Fig. 6*C*,*E*). This result raises two possibilities for the role of $GABA_A$-mediated inhibition: (1) it is required for the induction of heterosynaptic potentiation, or (2) the heterosynaptic potentiation we observe is actually due to the slow disinhibition of SC synaptic strength and we do not observe "potentiation" in these experiments because there is no inhibition to be lost. The second possibility is unlikely for two reasons. First, to measure our extracellular field potentials (Fig. 1), we measured the initial slope of the field PSP which is not contaminated by feedforward inhibition. Second, blocking intracellular Ca^{2+} elevation with BAPTA prevented heterosynaptic potentiation (Fig. 3). Still, to directly rule out a role for disinhibition in the expression of heterosynaptic potentiation, we gave SLM TBS in normal ACSF and quickly washed in SR95531. Because the kinetics of expression of heterosynaptic potentiation are slow, we were able to fully block $GABA_A$ receptors before any significant expression of heterosynaptic potentiation. We renormalized SC synaptic strength during this period (5–10 min after SLM TBS) and found that wash-in of SR95531 after SLM TBS did not block heterosynaptic potentiation (1.27 ± 0.07, $n = 9$, $p < 0.05$ compared to no SLM TBS, 0.99 ± 0.09, $n = 7$; Fig. 6*B*,*C*,*E*). Thus, we conclude that $GABA_A$ receptor-mediated inhibition is required for the induction of heterosynaptic potentiation.

Next we tested the contribution of several signaling pathways implicated in synaptic plasticity. We found that heterosynaptic potentiation did not depend on L-type Ca^{2+} channels (nimodipine, 1.23 ± 0.05, $n = 6$), Ca^{2+} release from internal stores (thapsigargin, 1.20 ± 0.08, $n = 4$), dopamine signaling through D_1/D_5 receptors (SCH23390, 1.19 ± 0.07, $n = 5$), muscarinic acetylcholine receptors (atropine, 1.31 ± 0.14, $n = 4$), or mGluR5 signaling (MPEP, 1.23 ± 0.10, $n = 5$; all conditions compared including SLM TBS with no inhibitors; $p = 0.99$ by Kruskal–Wallis test; Fig. 6*E*). To summarize, in marked contrast to homosynaptic LTP, the induction of heterosynaptic potentiation does not depend of NMDA receptors, but instead requires both R-/T-type Ca^{2+} channels and $GABA_A$ receptor-mediated inhibition.

Expression mechanisms of heterosynaptic potentiation

Paired-pulse ratio

While the induction mechanisms of heterosynaptic potentiation are distinct from LTP, how similar are their expression mechanisms? Homosynaptic LTP is believed to be postsynaptically expressed by the insertion of AMPA receptors, whereas NMDA receptor-mediated transmission remains unchanged. First we looked for changes in presynaptic function after heterosynaptic potentiation by using extracellular field recording to measure the paired-pulse ratio (PPR), an indicator of the presynaptic probability of transmitter release. We found that the PPR was not altered after heterosynaptic potentiation (SC PPR baseline, 1.60 ± 0.09 vs PPR at 50–60 min after TBS, 1.66 ± 0.06; $n = 4$, $p = 0.25$; Fig. 7*A*, left), while normal heterosynaptic potentiation was seen in these experiments (1.17 ± 0.05, $n = 4$; Fig. 7*A*, right), consistent with little or no change in the presynaptic probability of release. However, PPR is only an approximation for presynaptic function and does not always correlate with probability of release (Deng et al., 2011), so although our results are consistent with no presynaptic alterations, we cannot rule out the possibility that changes in presynaptic function contribute to heterosynaptic potentiation.

Occlusion by prior LTP

Next we examined how similar our AMPA receptor-mediated heterosynaptic potentiation was to homosynaptic AMPA receptor LTP by testing whether LTP could occlude the expression of heterosynaptic potentiation. To do this, we stimulated two independent SC pathways and saturated homosynaptic LTP in one pathway using a TBS protocol repeated four times at 5 min intervals, and then induced heterosynaptic potentiation by SLM TBS and looked for differences in heterosynaptic potentiation in the saturated and the naive pathways (Fig. 7*B*, top). For display purposes only, we renormalized synaptic strength in the saturated pathway to facilitate comparison to the naive pathway. SC LTP remained saturated throughout the experiment as another 4× TBS delivered to the saturated pathway at the conclusion of the experiment did not induce further LTP (data not shown). Control slices did not receive SLM TBS, and both SC pathways were stable until the end of the experiment (after renormalization, $SC_{saturated}$ at the end of the experiment, 1.02 ± 0.01 vs SC_{naive}, 1.04 ± 0.04; $n = 7$, $p = 0.61$; Fig. 7*B*, bottom left). SLM TBS

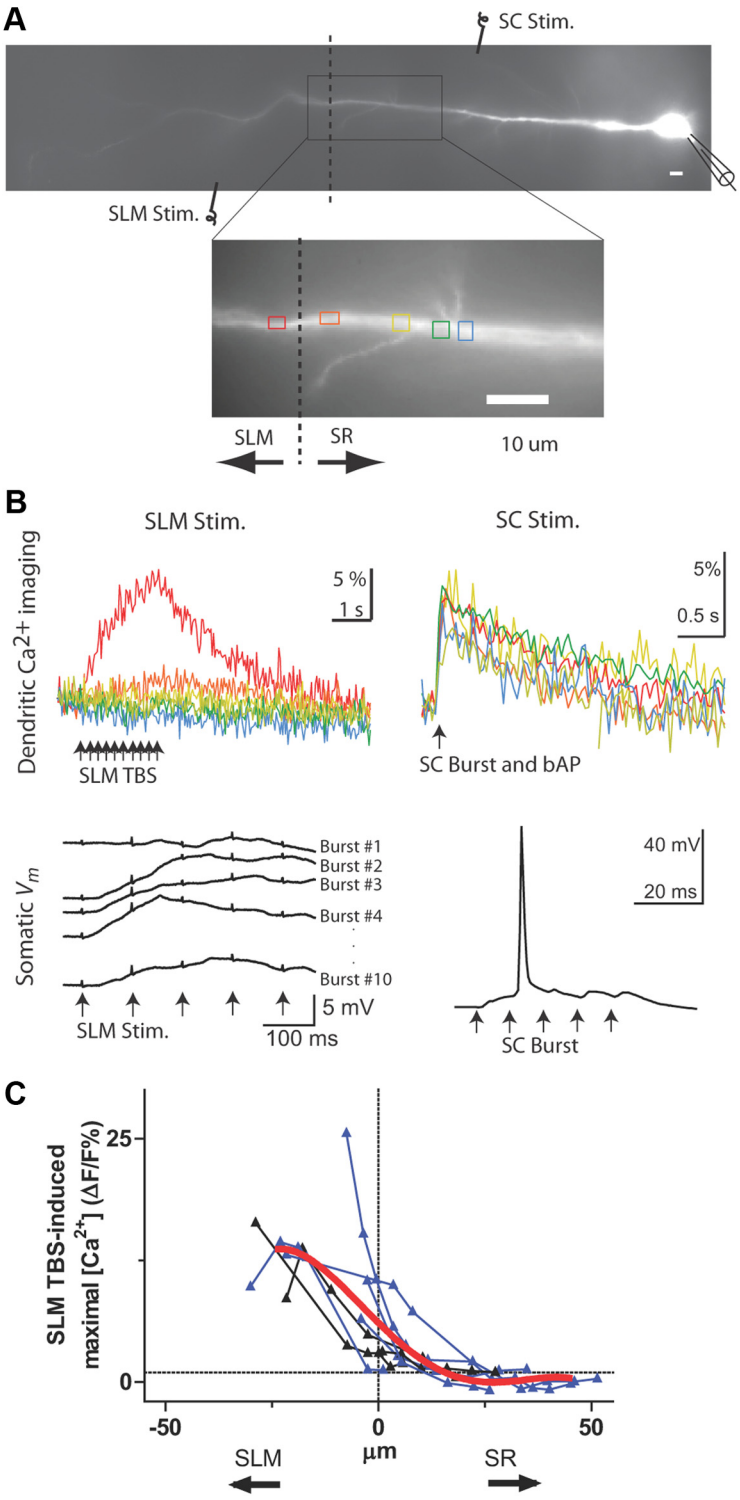

Figure 5. Large, spatially restricted Ca^{2+} transients are induced by SLM TBS. ***A***, Top, Low-magnification montage of an OGB-1-filled CA1 pyramidal neuron shown from the stratum pyramidale on the right to the hippocampal fissure on the left. The dotted line indicates the approximate border between the stratum radiatum and stratum lacunosum moleculare. Scale bar, 50 μm. Bottom, Field of view for Ca^{2+} imaging at the SLM/SR border. Colored boxes indicate windows for quantification of Ca^{2+} signal. ***B***, Top left, Dendritic Ca^{2+} ($\Delta F/F$) induced by SLM TBS. Color map corresponds to boxes in ***A***. Bottom left, Simultaneous V_m for SLM TBS measured at the soma. Traces are vertically offset for clarity. Top right, Dendritic Ca^{2+} induced by a single SC burst of five stimuli and associated backpropagating AP. Bottom right, Simultaneously recorded V_m at the soma. ***C***, Summary data of Ca^{2+} imaging from nine neurons using either OGB-1 (blue lines, $n = 6$) or Fluo-4 (black lines, $n = 3$). Triangles indicate quantification windows along each dendrite, with their locations plotted relative to the approximate SLM/SR border. Red line is the quadratic fit of all neurons ($R^2 = 0.65$).

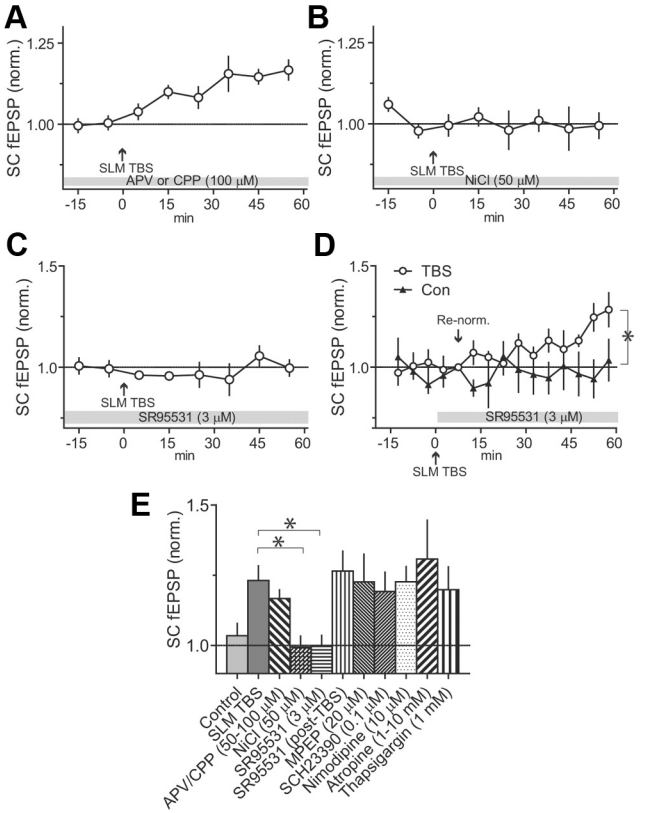

Figure 6. Heterosynaptic potentiation depends on $GABA_A$ receptor-mediated inhibition and R-/T-type Ca^{2+} channels. ***A***, D,L-APV or *R*-CPP did not affect the induction or expression of heterosynaptic plasticity. ***B***, Block of R-/T-type $Ca2^{+}$ channels by NiCl prevented heterosynaptic plasticity. ***C***, Block of $GABA_A$ receptor-mediated inhibition by SR95531 present throughout the experiment prevented heterosynaptic potentiation. ***D***, $GABA_A$ receptor-mediated inhibition is required for the induction of heterosynaptic potentiation. SR95531 was washed in immediately after SLM TBS. fEPSPs were renormalized after complete $GABA_A$ receptor block at 5–10 min after drug wash-in (down arrow). ***E***, SC potentiation at 50–60 min after SLM TBS under different pharmacological conditions. $*p < 0.05$.

induced normal heterosynaptic potentiation in the naive SC pathway, but heterosynaptic potentiation was significantly occluded by SC LTP in the saturated pathway (SC_{naive}, 1.23 ± 0.06 vs $SC_{saturated}$, 1.08 ± 0.03; $n = 6$, $p < 0.05$; Fig. 7*B*, bottom right). This occlusion suggests that heterosynaptic and homosynaptic AMPA receptor potentiation share some common expression mechanism. It remains unclear whether heterosynaptic potentiation depends on AMPA receptor insertion, or if potentiation is occluded at an earlier step in the signal transduction pathway.

AMPA/NMDA EPSC ratio after heterosynaptic potentiation

To further probe the relationship between heterosynaptic potentiation and homosynaptic LTP, we looked for changes in the AMPA/NMDA ratio. Homosynaptic SC LTP is characterized by an increase in the AMPA/NMDA ratio, reflecting the potentiation of AMPA receptor-mediated signaling, whereas NMDA receptor-mediated signaling is unchanged (Kauer et al., 1988). Since we found that the AMPA-receptor mediated heterosynaptic potentiation was occluded by homosynaptic LTP, we expected the AMPA/NMDA ratio to increase after heterosynaptic potentiation. We measured the AMPA/NMDA ratio by inducing heterosynaptic plasticity, and then after the expression of potentiation, patching an individual neuron and measuring the AMPA (at −70 mV) and NMDA (at +30 mV) components (Fig. 7*C*, top left). To our surprise, we found that the AMPA/NMDA ratio of peak EPSCs was unchanged after heterosynaptic potentiation (AMPA/NMDA ratio in control neurons, 5.49 ± 0.77, $n = 6$ vs after SLM TBS, 5.64 ± 0.62, $n = 5$; $p = 0.93$; Fig. 7*C*, right, top, bottom), suggesting that NMDA signaling had increased concomitantly with AMPA signaling.

NMDA receptor contribution to heterosynaptic potentiation

NMDA receptors consist of a mixture of GluN2A and GluN2B subunit-containing receptors, with GluN2A dominating in adult neurons (Monyer et al., 1992; Williams et al., 1993). Increased NMDA receptor signaling could be achieved by preferentially increasing current mediated either by GluN2A subunits, by GluN2B, or by scaling up the contribution of both subunits equally. We distinguished between these possibilities by recording synaptic NMDA currents and then washing in the GluN2B-specific antagonist ifenprodil (3 μM) (Williams et al., 1993). Ifenprodil had little effect on NMDA EPSC peak current and area in control slices, inhibiting 10.84 ± 3.87% and 10.36 ± 5.28%, respectively ($n = 6$; Fig. 8*A*, *C*), consistent with the downregulation of this receptor subunit in mature animals. In contrast, neurons that received SLM TBS showed increased sensitivity to ifenprodil, with NMDA peak current inhibition of 33.78 ± 7.30% and NMDA area inhibition of 37.67 ± 6.26% ($n = 5$), significantly more inhibited by ifenprodil than control slices ($p < 0.05$; Fig. 8*B*, *C*). These data show that NMDA receptor signaling at SC synapses is shifted after stimulation of the direct cortical inputs, from a mature, GluN2A-dominated NMDA current to a more juvenile composition with significant contribution from GluN2B-containing receptors.

To summarize, the expression of heterosynaptic potentiation consists of both AMPA and NMDA receptor-mediated components. The AMPA receptor-mediated component is postsynaptic and occluded by previous homosynaptic LTP, suggesting shared expression mechanisms. However, unlike homosynaptic LTP, heterosynaptic potentiation has an additional NMDA receptor-mediated component, specifically, the increased contribution of juvenile GluN2B subunits in these mature mice.

These findings predict opposite metaplastic effects of heterosynaptic plasticity on subsequent SC signaling. On the one hand, the increase in synaptic GluN2B predicts a greater magnitude of SC LTP (Kirkwood et al., 1996) via greater Ca^{2+} influx and coupling to downstream effectors (Barria and Malinow, 2005; Sobczyk et al., 2005). On the other hand, homosynaptic SC LTP occludes heterosynaptic potentiation (Fig. 7*B*), suggesting less SC LTP after heterosynaptic potentiation. We hypothesized that these two effects might be differentially engaged as a function of SC stimulus intensity and tested this prediction using either weak (one TBS of 30 stimuli) or strong stimulation (four TBS at 5 min intervals, 50 stimuli per burst, 200 stimuli total) to trigger homosynaptic SC LTP after prior heterosynaptic potentiation. In control slices that did not receive SLM TBS, we found that the weak TBS protocol produced stable SC LTP (1.20 ± 0.04, $n = 6$; Fig. 9*A*). In slices that received SLM TBS, heterosynaptic potentiation developed normally (1.15 ± 0.04, $n = 7$ vs controls, 1.01 ± 0.03, $n = 6$; $p < 0.05$); however, subsequent weak TBS produced LTP that was significantly occluded (1.03 ± 0.02, $n = 6$, $p = 0.01$; Fig. 9*A*), consistent with the occlusion seen in Figure 7*B*, where SC LTP was expressed before heterosynaptic plasticity.

In marked contrast, when SC LTP was induced using the strong TBS protocol, SC LTP was significantly larger in slices that had undergone prior heterosynaptic plasticity compared to LTP from control slices (control LTP, 1.25 ± 0.03, $n = 10$ vs LTP after SLM TBS, 1.45 ± 0.05, $n = 10$; $p < 0.01$ by Kruskal–Wallis; $p <$

0.05 by Dunn's multiple comparison; Fig. 9*B*). Enhanced SC LTP in slices after heterosynaptic plasticity was dependent on the activity of GluN2B-containing NMDA receptors, as blocking these receptors with ifenprodil before SC TBS decreased LTP to 1.12 ± 0.06 ($n = 6$), significantly smaller than LTP in untreated SLM TBS slices ($p < 0.01$ by Dunn's multiple comparison; Fig. 9*B*). Ifenprodil itself had no effect on SC LTP in control slices (control LTP, 1.25 ± 0.01, $n = 6$ vs LTP with ifenprodil, 1.26 ± 0.08, $n = 4$; $p = 0.91$; Fig. 9*C*).

To illustrate the differential effects of heterosynaptic plasticity on moderate and strong SC stimulation, we plotted the amount of LTP versus the number of stimulations in the SC theta burst (Fig. 9*D*, left). The resulting graph clearly shows that heterosynaptic plasticity inhibits SC LTP induced by moderate SC stimulation, while a longer and repeated TBS protocol results in larger SC LTP. Plotting the effects of heterosynaptic plasticity as the percentage of inhibition or enhancement of SC LTP further demonstrates that prior heterosynaptic plasticity inhibited SC LTP induced by moderate SC TBS by 84.18%, but increased SC LTP by 77.38% when induced by strong SC TBS (Fig. 9*D*, right). These data highlight the powerful metaplastic control that heterosynaptic plasticity exerts over subsequent SC LTP.

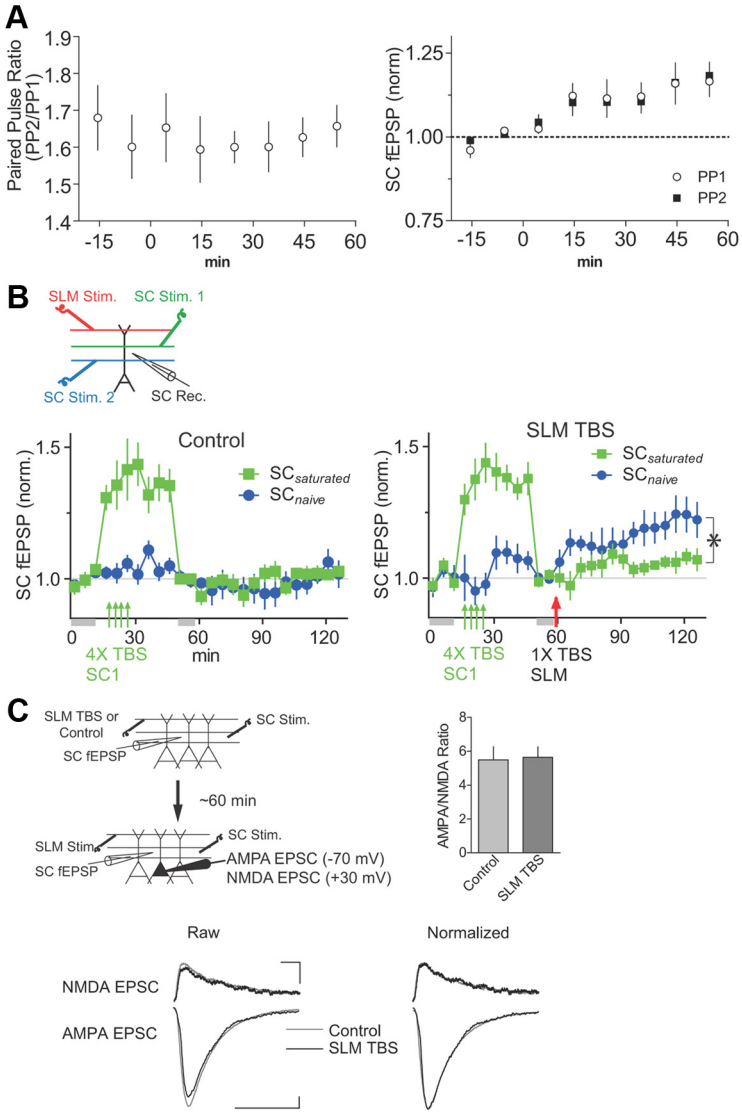

Figure 7. Expression of heterosynaptic potentiation. No change in paired-pulse ratio consistent with postsynaptic expression of heterosynaptic potentiation. ***A***, Left, Paired-pulse ratio measured by extracellular field recordings of SC fEPSP after SLM TBS. Right, Paired pulse 1 (PP1) versus paired pulse 2 (PP2) showing normal heterosynaptic potentiation. ***B***, AMPA receptor-mediated heterosynaptic potentiation is occluded by homosynaptic potentiation. Top, Schematic of occlusion experiment. LTP is saturated in $SC_{saturated}$ by repeating the TBS protocol four times at 5 min intervals. Bottom left, Control slices did not receive SLM TBS. After saturation of $SC_{saturated}$ by LTP (black arrows), fEPSPs were renormalized for display purposes only, to facilitate comparison to SC_{naive} (normalization denoted by gray bars). Bottom right, Comparison of $SC_{saturated}$ and SC_{naive} in slices that received an SLM TBS. ***C***, No change in AMPA/NMDA ratio after heterosynaptic potentiation. Top left, After the induction and expression of heterosynaptic potentiation, we washed in SR95531 and patched a neuron to measure the AMPA and NMDA receptor-mediated EPSC. Top right, Comparison of AMPA/NMDA ratio in control slices and SLM TBS slices >60 min after induction. Bottom left, Traces of average AMPA and NMDA receptor EPSCs from two cells, including one that had undergone SLM TBS-induced heterosynaptic potentiation. Calibration: NMDA EPSC, 50 pA, 25 ms; AMPA EPSC, 15 pA, 25 ms. Bottom right, Traces from control and SLM TBS neurons after normalization to AMPA receptor EPSC. *$p < 0.05$.

Discussion

Our current understanding of distal apical tuft synapses is that their main function is to modulate time-locked proximal input (Remondes and Schuman, 2002; Jarsky et al., 2005; Takahashi and Magee, 2009). We show that strong distal synaptic activation alone has long-lasting effects on neuronal activity through heterosynaptic potentiation of proximal synapses. This heterosynaptic potentiation is expressed by both increased AMPA and NMDA receptor-mediated synaptic strength, the latter specifically by enhanced GluN2B signaling. Furthermore we demonstrate that these two mechanisms interact to both shift the input selectivity of SC synapses and expand the dynamic range of LTP. This finding reveals a new organizational level for the regulation of synapses and circuit function: pathway-specific control of synaptic strength where signals at distal inputs can produce long-lasting modulation of proximal synapses.

Heterosynaptic plasticity has been observed in diverse preparations and can be expressed in various forms. Many types of heterosynaptic plasticity act to homeostatically regulate synaptic strength; for example, homosynaptic LTP can result in heterosynaptic LTD at nearby nonstimulated synapses (Nishiyama et al., 2000; Royer and Paré, 2003; Chevaleyre and Castillo, 2004). However, the opposite is also seen where homosynaptic potentiation results in heterosynaptic potentiation (Engert and Bonhoeffer, 1997; Reissner et al., 2010). One common characteristic of previously described forms of heterosynaptic plasticity is the short spatial spread of heterosynaptic effects, on the order of tens of microns. This is due to the nature of the induction signal for these forms of plasticity: the short-range diffusion of signaling molecules like endocannabinoids or the intracellular release of Ca^{2+} from internal stores. Functionally, these forms of heterosynaptic plasticity indiscriminately modify nearby synapses, favoring the coregulation of clustered groups of synapses. In con-

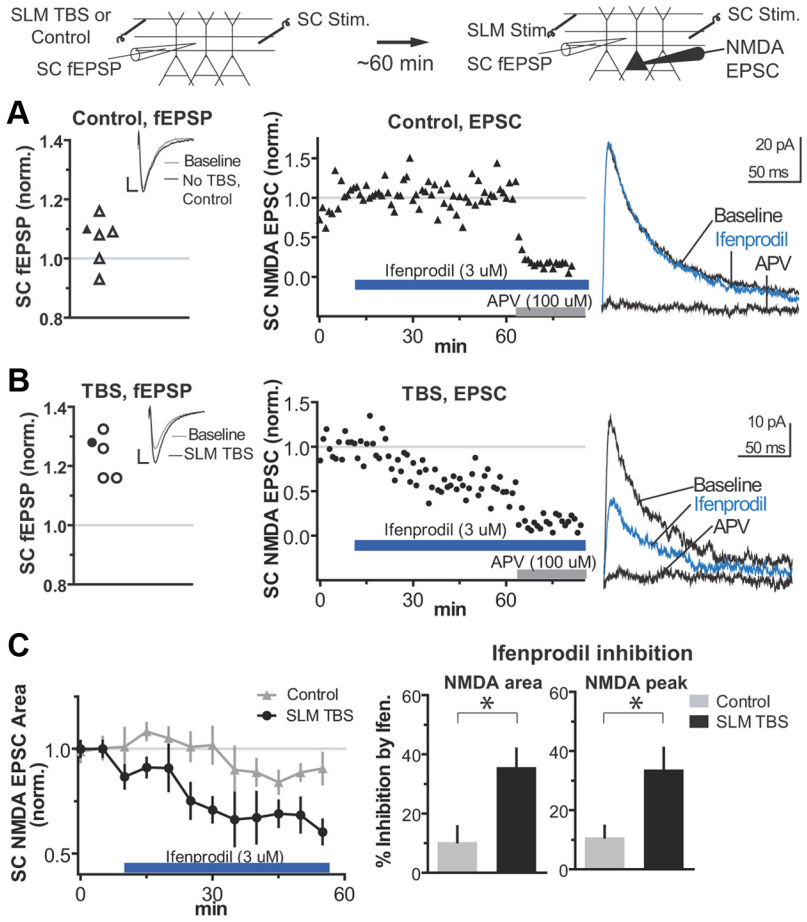

Figure 8. Heterosynaptic increase in synaptic GluN2B-mediated NMDA current. Top, Schematic of experiment. Heterosynaptic potentiation is induced during extracellular recording. Then an individual neuron is patched after expression of heterosynaptic potentiation, and the NMDA EPSC is measured. ***A***, Left, the fEPSP of each control slice 60 min after sham TBS, before recording NMDA currents. The filled symbol represents the slice shown in the middle and right panels. Inset, Averaged traces from the sample slice. Middle, An individual neuron was patched in SR95531 (10 μM) and NBQX (10 μM) and held at +30 mV to isolate NMDA receptor-mediated EPSC peaks in response to SC synaptic stimulation. Ifenprodil (3 μM) was washed in to block GluN2B-containing NMDA receptors and then D,L-APV (100 μM) to verify that currents were NMDA receptor dependent. Right, Averaged traces of baseline, ifenprodil-blocked, and APV-blocked currents. ***B***, Left, fEPSPs of slices 60 min after SLM TBS. Middle, Time course of drug wash-in for a single neuron. Right, Averaged traces. ***C***, Left, Time course of inhibition of NMDA EPSC areas by ifenprodil for the average of all control and SLM TBS neurons for a single neuron. Right, Inhibition of NMDA peaks and area by ifenprodil for control and SLM TBS neurons. *$p < 0.05$. Calibrations: ***A***, ***B***, Insets, 0.05 mV, 5 ms.

trast, the heterosynaptic plasticity we describe works across a much longer spatial scale and is both directional and input specific; that is, induction at one set of inputs can influence another set of anatomically and functionally distinct inputs. In this way, activity in the entorhinal cortex can act as a switch to control information flow within the hippocampus.

The cellular/molecular mechanisms underlying this plasticity remain unknown, although there are two scenarios by which activation of distal synapses could potentiate proximal synapses. First is the possibility that dendritic spikes, generated in the apical tuft, propagate some distance into the proximal dendrite to trigger plasticity directly at SC synapses. However, our Ca^{2+} imaging experiments showing that SLM-evoked Ca^{2+} signals drop precipitously at the SLM/SR border suggest that local activation of SC synapses is not likely. In addition, the long latency for the expression of heterosynaptic potentiation further argues against direct Ca^{2+}-dependent activation of SC synapses. Second is the possible activation of a signaling molecule in the distal dendrite that diffuses or is transported proximally to generate plasticity. This scenario is compatible with the slow time course for heterosynaptic potentiation, but if this is the case, there must exist a yet unknown mechanism for preventing potentiation at SLM synapses or targeting the putative activation factor specifically to SC synapses. Examining heterosynaptic potentiation with single-synapse resolution to precisely define the spatiotemporal dynamics of potentiation will greatly aid in answering these questions.

While we have shown that intracellular Ca^{2+} is required for heterosynaptic potentiation, the role of dendritic spikes in the apical tuft remains unclear. Ca^{2+} imaging shows that the SLM stimulation protocol used for inducing heterosynaptic plasticity produces large Ca^{2+} transients in the apical tufts, but we have not shown that these transients result from supralinear summation of synaptic inputs. One intriguing possibility is that SLM stimulation strong enough to repeatedly drive dendritic spikes is required for the induction of heterosynaptic plasticity. Future experiments varying SLM activation while measuring dendritic spikes and subsequent heterosynaptic plasticity should resolve this possibility.

Another unusual aspect of this heterosynaptic plasticity is its dependence on $GABA_A$ receptor-mediated inhibition. There are at least two possibilities for the role of inhibition in the induction of heterosynaptic potentiation. One is that $GABA_A$ receptor-mediated hyperpolarization may be required to deinactivate low-threshold-activated T-type calcium channels located in the apical tuft, and the resulting rebound firing after the release of inhibition is required for generating large Ca^{2+} transients. This possibility is consistent with our result showing that R- or T-type Ca^{2+} channels are required for heterosynaptic potentiation. Continued pharmacological dissection of the contribution of these two types of calcium channels will resolve this possibility. Second, it has been shown that presynaptic $GABA_A$ receptors can unexpectedly enhance LTP induction by depolarizing the synaptic terminal in hippocampal mossy fiber boutons (Nakamura et al., 2007; Ruiz et al., 2010). Further work will be required to reveal exactly how $GABA_A$ receptor-mediated inhibition contributes to the induction of heterosynaptic plasticity. Although we ruled out the contribution of many molecular pathways to heterosynaptic potentiation (Fig. 6*E*), we did not exhaustively test all possibilities. In particular, we did not investigate the role of $GABA_B$ inhibition, which has been shown to mediate cross-pathway inhibition at these synapses on a millisecond-to-second time scale (Dvorak-Carbone and Schuman, 1999). It remains to be seen what role, if any, it plays in long-lasting heterosynaptic changes.

The heterosynaptic plasticity we describe is distinct from, and strikingly complementary to, Hebbian LTP. While LTP expresses quickly with no change in NMDA receptor-mediated current,

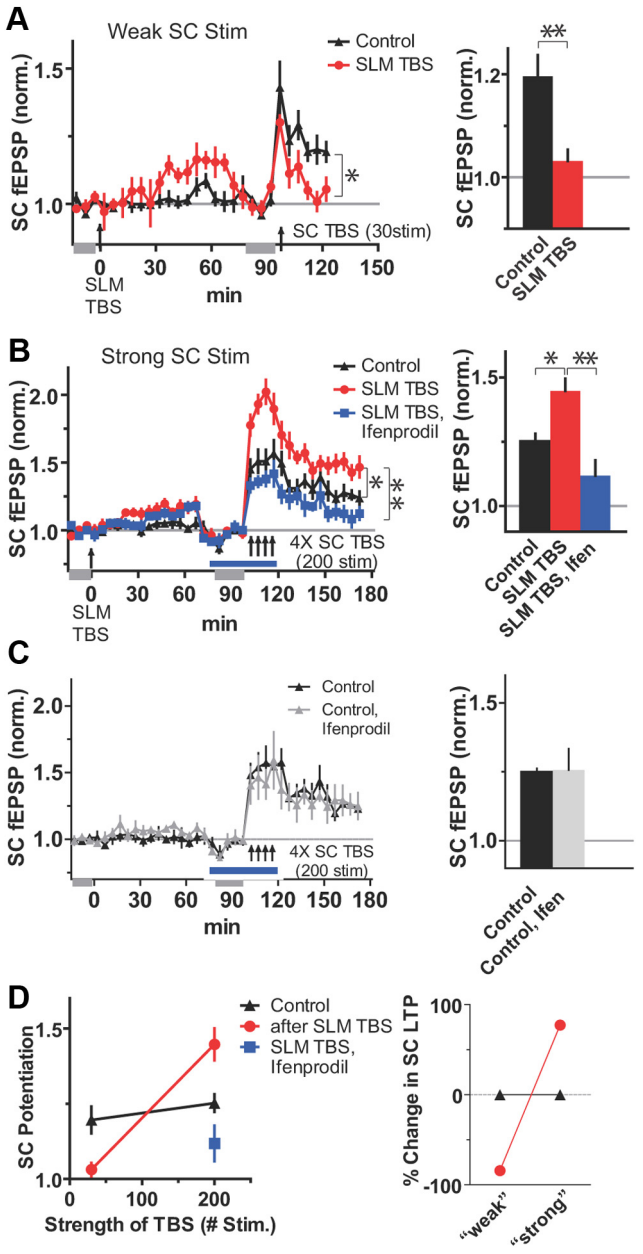

Figure 9. Heterosynaptic plasticity inhibits subsequent SC LTP induced by mild SC stimulation but enhances LTP induced by strong SC stimulation. ***A***, Left, Slices received either SLM TBS or no stimulation (controls) at $t = 0$. At $t = 70$ min, stimulus intensity was turned down to match baseline levels, and fEPSPs were renormalized (gray bars). Slices received a single SC TBS (3 stimuli at 100 Hz, repeated 10 times at 5 Hz). Right, Average SC LTP at 20–30 min after a single SC TBS. ***B***, Left, Slices received a stronger SC TBS (5 stimuli at 100 Hz, repeated 10 times at 5 Hz) repeated four times at 5 min intervals. Ifenprodil (3 μM) was present (blue bar) for the "SLM TBS, Ifenprodil" condition. Right, Average SC LTP at 50–60 min after strong SC TBS. ***C***, Ifenprodil does not affect control LTP. Slices with or without ifenprodil present during the induction of SC LTP by 4× TBS are shown. ***D***, Left, Values for SC LTP from ***A*** and ***B***, plotted as a function of number of stimulations in the SC TBS. Right, SC LTP in slices after heterosynaptic plasticity normalized to levels of LTP in control slices. *$p < 0.05$; **$p < 0.01$.

heterosynaptic plasticity develops slowly and features a metaplastic shift of NMDA receptor subunits. Computational modeling of neuronal networks has found that engaging multiple plasticity mechanisms featuring this specific combination of offset time courses coupled with metaplastic modification of synapses dramatically improves memory retention by preventing interference between plasticity mechanisms (Fusi et al., 2005). Thus, while the fast time course of LTP is well suited for the rapid encoding of memories, slow heterosynaptic plasticity may come online to capture a later phase of memory formation. If heterosynaptic plasticity does contribute to memory encoding, its distinctly slow kinetics should be observable in the development of CA1 firing *in vivo*. Indeed, several studies have found that although CA3 firing rates stabilize within minutes after an animal has been introduced to a new environment, CA1 firing continues to evolve over hours to days (Lever et al., 2002; Leutgeb, 2006; Karlsson and Frank, 2008; Dupret et al., 2010).

How might memory be encoded in heterosynaptically activated neurons? One specific form of network activity that is uniquely suited to match these dual requirements for delayed activation and strong, repeated afferent input is sharp wave/ripple complexes. These events, believed to drive memory consolidation, occur constantly during pauses in active exploration and slow-wave sleep and are associated with the repeated replay of previous experience (Lee and Wilson, 2002; Girardeau et al., 2009; Nakashiba et al., 2009; Dupret et al., 2010; Jadhav et al., 2012). Furthermore, sharp waves/ripples, generated by the intense, synchronized discharge of CA3 neurons, are the strongest known form of hippocampal network depolarization, driving firing in CA1 neurons and activity throughout the cortex (Buzsáki, 1986; Siapas and Wilson, 1998; Ji and Wilson, 2007). Thus, strong entorhinal cortical input activating heterosynaptic plasticity may prime an ensemble of CA1 neurons for memory consolidation via sharp wave/ripples occurring during exploration or sleep. This proposed role for heterosynaptic plasticity in memory consolidation is consistent with a study showing that lesion of the direct entorhinal cortical pathway to the distal dendrites of CA1 prevented memory consolidation (Remondes and Schuman, 2004).

Synaptic inputs onto electrotonically remote distal dendritic tufts occur throughout the brain, raising the possibility that heterosynaptic plasticity may operate in other neuron types. Unfortunately, the lack of well-segregated afferent input in other brain regions and the washout of plasticity during whole-cell recording make studying this plasticity difficult. However, the use of the repatch technique described here combined with optogenetic stimulation of defined afferent inputs should reveal whether heterosynaptic plasticity is a common signaling mechanism for distal dendritic synapses.

References

Barria A, Malinow R (2005) NMDA receptor subunit composition controls synaptic plasticity by regulating binding to CaMKII. Neuron 48:289–301. CrossRef Medline

Buzsáki G (1986) Hippocampal sharp waves: their origin and significance. Brain Res 398:242–252. CrossRef Medline

Chevaleyre V, Castillo PE (2004) Endocannabinoid-mediated metaplasticity in the hippocampus. Neuron 43:871–881. CrossRef Medline

Deng PY, Sojka D, Klyachko VA (2011) Abnormal presynaptic short-term plasticity and information processing in a mouse model of Fragile X syndrome. J Neurosci 31:10971–10982. CrossRef Medline

Dudman JT, Tsay D, Siegelbaum SA (2007) A role for synaptic inputs at distal dendrites: instructive signals for hippocampal long-term plasticity. Neuron 56:866–879. CrossRef Medline

Dupret D, O'Neill J, Pleydell-Bouverie B, Csicsvari J (2010) The reorganization and reactivation of hippocampal maps predict spatial memory performance. Nat Neurosci 13:995–1002. CrossRef Medline

Dvorak-Carbone H, Schuman EM (1999) Patterned activity in stratum lacunosum moleculare inhibits CA1 pyramidal neuron firing. J Neurophysiol 82:3213–3222. Medline

Engert F, Bonhoeffer T (1997) Synapse specificity of long-term potentiation breaks down at short distances. Nature [Erratum (1997) 388:698] 388:279–284. CrossRef Medline

Fusi S, Drew PJ, Abbott LF (2005) Cascade models of synaptically stored memories. Neuron 45:599–611. CrossRef Medline

Fyhn M, Hafting T, Witter MP, Moser EI, Moser MB (2008) Grid cells in mice. Hippocampus 18:1230–1238. CrossRef Medline

Girardeau G, Benchenane K, Wiener SI, Buzsáki G, Zugaro MB (2009) Selective suppression of hippocampal ripples impairs spatial memory. Nat Neurosci 12:1222–1223. CrossRef Medline

Golding NL, Spruston N (1998) Dendritic sodium spikes are variable triggers of axonal action potentials in hippocampal CA1 pyramidal neurons. Neuron 21:1189–1200. CrossRef Medline

Golding NL, Staff NP, Spruston N (2002) Dendritic spikes as a mechanism for cooperative long-term potentiation. Nature 418:326–331. CrossRef Medline

Hargreaves EL, Rao G, Lee I, Knierim JJ (2005) Major dissociation between medial and lateral entorhinal input to dorsal hippocampus. Science 308: 1792–1794. CrossRef Medline

Izumi Y, Tokuda K, Zorumski CF (2008) Long-term potentiation inhibition by low-level N-methyl-D-aspartate receptor activation involves calcineurin, nitric oxide, and p38 mitogen-activated protein kinase. Hippocampus 18:258–265. CrossRef Medline

Jadhav SP, Kemere C, German PW, Frank LM (2012) Awake hippocampal sharp-wave ripples support spatial memory. Science 336:1454–1458. CrossRef Medline

Jarsky T, Roxin A, Kath WL, Spruston N (2005) Conditional dendritic spike propagation following distal synaptic activation of hippocampal CA1 pyramidal neurons. Nat Neurosci 8:1667–1676. CrossRef Medline

Ji D, Wilson MA (2007) Coordinated memory replay in the visual cortex and hippocampus during sleep. Nat Neurosci 10:100–107. CrossRef Medline

Karlsson MP, Frank LM (2008) Network dynamics underlying the formation of sparse, informative representations in the hippocampus. J Neurosci 28:14271–14281. CrossRef Medline

Kauer JA, Malenka RC, Nicoll RA (1988) A persistent postsynaptic modification mediates long-term potentiation in the hippocampus. Neuron 1:911–917. CrossRef Medline

Kirkwood A, Rioult MC, Bear MF (1996) Experience-dependent modification of synaptic plasticity on visual cortex. Nature 381:526–528. CrossRef Medline

Larkum ME, Zhu JJ, Sakmann B (1999) A new cellular mechanism for coupling inputs arriving at different cortical layers 398:338–341.

Lee AK, Wilson MA (2002) Memory of sequential experience in the hippocampus during slow wave sleep. Neuron 36:1183–1194. CrossRef Medline

Leutgeb S, Leutgeb JK, Moser EI, Moser MB (2006) Fast rate coding in hippocampal CA3 cell ensembles. Hippocampus 16:765–774. CrossRef Medline

Lever C, Wills T, Cacucci F, Burgess N, O'Keefe J (2002) Long-term plasticity in hippocampal place-cell representation of environmental geometry. Nature 416:90–94. CrossRef Medline

Malenka RC, Kauer JA, Zucker RS, Nicoll RA (1988) Postsynaptic calcium is sufficient for potentiation of hippocampal slice transmission. Science 242: 81–84. CrossRef Medline

Monyer H, Sprengel R, Schoepfer R, Herb A, Higuchi M, Lomeli H, Burnashev N, Sakmann B, Seeburg PH (1992) Heteromeric NMDA receptors: molecular and functional distinction of subtypes. Science 256:1217–1221. CrossRef Medline

Morris RG, Anderson E, Lynch GS, Baudry M (1986) Selective impairment of learning and blockade of long-term potentiation by an N-methyl-D-aspartate receptor antagonist, AP5. Nature 319:774–776. CrossRef Medline

Nakamura M, Sekino Y, Manabe T (2007) GABAergic interneurons facilitate mossy fiber excitability in the developing hippocampus. J Neurosci 27:1365–1373. CrossRef Medline

Nakashiba T, Buhl DL, McHugh TJ, Tonegawa S (2009) Hippocampal CA3 output is crucial for ripple-associated reactivation and consolidation of memory. Neuron 62:781–787. CrossRef Medline

Nishiyama M, Hong K, Mikoshiba K, Poo MM, Kato K (2000) Calcium stores regulate the polarity and input specificity of synaptic modification. Nature 408:584–588. CrossRef Medline

Otmakhova NA, Otmakhov N, Lisman JE (2002) Pathway-specific properties of AMPA and NMDA-mediated transmission in CA1 hippocampal pyramidal cells. J Neurosci 22:1199–1207. Medline

Reissner KJ, Pu L, Schaffhausen JH, Boyle HD, Smith IF, Parker I, Carew TJ (2010) A novel postsynaptic mechanism for heterosynaptic sharing of short-term plasticity. J Neurosci 30:8797–8806. CrossRef Medline

Remondes M, Schuman EM (2002) Direct cortical input modulates plasticity and spiking in CA1 pyramidal neurons. Nature 416:736–740. CrossRef Medline

Remondes M, Schuman EM (2004) Role for a cortical input to hippocampal area CA1 in the consolidation of a long-term memory. Nature 431:699–703. CrossRef Medline

Royer S, Paré D (2003) Conservation of total synaptic weight through balanced synaptic depression and potentiation. Nature 422:518–522. CrossRef Medline

Ruiz A, Campanac E, Scott RS, Rusakov DA, Kullmann DM (2010) Presynaptic GABAA receptors enhance transmission and LTP induction at hippocampal mossy fiber synapses. Nat Neurosci 13:431–438. CrossRef Medline

Sargolini F, Fyhn M, Hafting T, McNaughton BL, Witter MP, Moser MB, Moser EI (2006) Conjunctive representation of position, direction, and velocity in entorhinal cortex. Science 312:758–762. CrossRef Medline

Schiller J, Schiller Y, Stuart G, Sakmann B (1997) Calcium action potentials restricted to distal apical dendrites of rat neocortical pyramidal neurons. J Physiol 505:605–616. CrossRef Medline

Siapas AG, Wilson MA (1998) Coordinated interactions between hippocampal ripples and cortical spindles during slow-wave sleep. Neuron 21:1123–1128. CrossRef Medline

Sobczyk A, Scheuss V, Svoboda K (2005) NMDA receptor subunit-dependent [Ca2+] signaling in individual hippocampal dendritic spines. J Neurosci 25:6037–6046. CrossRef Medline

Takahashi H, Magee JC (2009) Pathway interactions and synaptic plasticity in the dendritic tuft regions of CA1 pyramidal neurons. Neuron 62:102–111. CrossRef Medline

Williams K, Russell SL, Shen YM, Molinoff PB (1993) Developmental switch in the expression of NMDA receptors occurs *in vivo* and *in vitro*. Neuron 10:267–278. CrossRef Medline

Wöhrl R, von Haebler D, Heinemann U (2007) Low-frequency stimulation of the direct cortical input to area CA1 induces homosynaptic LTD and heterosynaptic LTP in the rat hippocampal-entorhinal cortex slice preparation. Eur J Neurosci 25:251–258. CrossRef Medline

Wouterlood FG, Saldana E, Witter MP (1990) Projection from the nucleus reuniens thalami to the hippocampal region: light and electron microscopic tracing study in the rat with the anterograde tracer *Phaseolus vulgaris*-leucoagglutinin. J Comp Neurol 296:179–203. CrossRef Medline